Buoyancy-dominated laminar convection and radiation transfer in rod arrays

A. K. Mohanty* and R. Viskanta†

Laminar combined free and forced convection together with radiation transfer in flow of steam at 68 bar through rods in triangular and square arrays have been investigated numerically. The pitch to diameter ratio has been varied from 1.2 to 2.0. Heat transfer results have been obtained for both up and down forced flow influenced by buoyancy with and without the effects of variable thermophysical fluid properties. The Rosseland diffusion approximation has been used for radiative transfer. First- and second-order density changes have been investigated.

Keywords: *heat transfer, combined convection, radiation, rod arrays*

Introduction

Recent interest in studies of rod-bundle heat transfer stem from the need to predict the thermal hydraulic performance of nuclear reactors in the event of a severe transient such as a loss of coolant accident (LOCA). Postaccident investigations[1-3] have led to reconstruction of the transient scenario that can be used for increasingly realistic modeling of the LOCA-related thermal hydraulic studies. A closer modeling, however, needs a complementary heat transfer database.

Consider the situation prevailing in a partly uncovered nuclear reactor core. The system pressure would have decreased to a level, for example, 68 bar, in case of the TMI-2 depending on the duration the pressure-operated relief valve (PORV) remained (stuck) open. The steam generated at the froth (two-phase mixture) level would move upward along the rod channels but it would be influenced significantly by buoyancy. The rod to steam temperature difference could be so high as to additionally cause radiation to be a significant mode of heat exchange.[3]

With longer heights of uncovered core, the cladding temperature may exceed the threshold limit of oxidation and react with the steam. Significant oxidation of the cladding can cause ballooning and degradation of Zircaloy cladding even before the fuel elements reach their melting temperature.[4]

An analysis of cladding oxidation, therefore, requires steam heat transfer coefficient data that takes into account (1) the rod-bundle geometry; (2) high system pressure, nominally 68 bar; (3) variation of thermophysical properties with temperature at the prevailing system pressure; (4) combined free and forced convection as well as radiation transfer; and (5) the possibility that the rod to steam temperature difference could be too high to permit Boussinesq's assumption to remain valid.

Needless to say, transport rates satisying these requirements are not available in the literature. Under the circumstance, the reported thermal-hydraulic studies have assumed[5,6] the square array rod-bundle geometry to be an annulus whose outer boundary is made up of the interrod symmetry lines and whose center is occupied by a fuel rod. Fully developed laminar or turbulent forced convection heat transfer coefficients for the so imagined annulus are then used as the input model parameter.

At a high temperature, when the Zircaloy cladding reacts with steam, the steam is depleted, and hydrogen is generated, resulting in a change in the thermophysical properties of the coolant mixture. This, however, would not occur at all heights of the uncovered core but only at locations where the cladding temperature has exceeded the oxidation threshold value. Estimates of hydrogen generation have to be made by analyzing combined heat and mass transfer along the length of a fuel rod using appropriate transport rates.

The earliest studies[7,8] of rod-bundle heat transfer date back to 1959. The studies have been carried out for two types of geometries: infinite or simply connected and finite or multiply connected, the latter being pertinent to smaller-sized reactors. Much of the information available until 1977 was summarized by Shah and London[9] and updated through 1982 by Kakac *et al.*[10]

To date, analysis of heat transfer in rod bundles has been mostly limited to constant property fluids, the attention being focused on modeling the complex geometries. Studies of laminar combined free and forced convection in upward flow through triangular and square array of rods were first reported by Iqbal *et al.*,[11] who subsequently have considered a conjugate analysis.[12] Ramm and Johannsen[13] focused on the strong influence the buoyancy and power-skew can cause in inverting the temperature and velocity profiles in flow through rod bundles. Yang[14,15] showed the quantitative influence of buoyancy in decreasing heat transfer and increasing resistance in downward flow through triangular and square rod arrays.

More recently, Das and Mohanty[16] have reported on a combined free and forced convection heat transfer study for both upward flow and downward flow in finite bundles. The influence of power-skew and the ratio Gr/Re on heat transfer, friction factor, separation, and flow reversal has been demonstrated. Recently, Zhong *et al.*[17] pointed out the inadequacies of Boussinesq's assumption and have suggested an upper limit of temperature difference for the approximation to be valid.

In this study, we try to generate the transport rate coefficients in the transverse direction, complying with the five conditions identified earlier, for rods arranged in triangular and square arrays. The results so generated can then be used to study Zircaloy cladding oxidation along the length of a fuel rod. Laminar flow regime is considered in view of the fact that forced flow is practically depleted following a LOCA.

Analysis

Physical model

Fuel rods in a vertical configuration are considered arranged in a reactor core in triangular or square arrays. Shell-wall effects are discounted, and an array is divided into several identical subchannels: six of included angle $\theta_0 = 30°$ in a triangular array and four of $\theta_0 = 45°$ in a square array. Distance between two adjacent rods is defined through pitch P.

A subchannel has AB, BC, and CD as the symmetry lines across which the velocity and temperature gradients are zero

* Indian Institute of Technology, Kharagpur, 721302 India
† Purdue University, W. Lafayette, Indiana, 47907 U.S.A.
Received 10 October 1985 and accepted for publication 23 April 1986

0142-727X/87/040277-10$03.00

(Figure 1). The sector AD of the rod surface dissipates heat at a uniform flux q.

Governing equations

We assume fully developed hydrodynamic and thermal conditions and write the laminar momentum equation as

$$0=-\frac{dp_d}{dx}-\frac{dp_s}{dx}+\nabla\cdot(\mu\nabla u)\pm\rho g \tag{1}$$

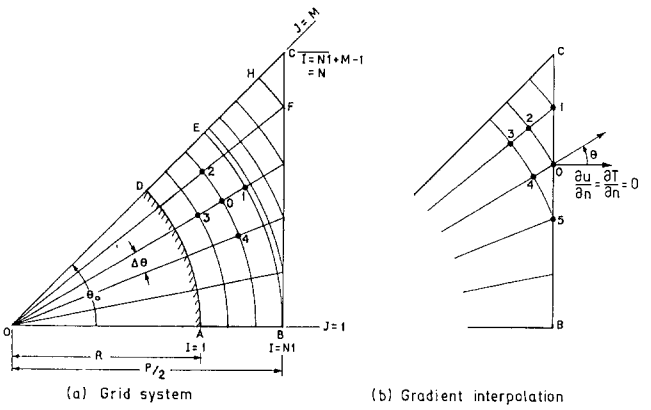

Figure 1 Physical model

where the + sign for the body force term applies to downward flow, and the − sign applies to upward flow. In Eq. (1), ρ_0 and β_0 are defined at a reference temperature T_0 for evaluating the static pressure gradient and the buoyancy terms. Thus

$$-\frac{dp_s}{dx}\pm\rho g=\pm(\rho-\rho_0)g \tag{2}$$

Second-degree correction to density due to temperature variations can be expressed through

$$\rho=\rho_0+\left(\frac{\partial\rho}{\partial T}\right)_p\Delta T+\frac{1}{2}\left(\frac{\partial^2\rho}{\partial T^2}\right)_p\Delta T^2 \tag{3}$$

where $\Delta T=T-T_0$. Using the definition $\beta=-(1/\rho)(\partial\rho/\partial T)|_p$ and noting $\beta\approx 1/T$, we obtain $\partial^2\rho/\partial T^2=2\beta^2\rho$. Hence from Eq. (3), it follows that

$$\frac{\rho-\rho_0}{\rho_0}=-\beta_0\Delta T(1-\beta_0\Delta T) \tag{4}$$

accounts for second-order density variation. If the analysis were restricted to Boussinesq's assumption, the term in parentheses would be equal to unity.

Substituting Eqs. (2) and (4) into Eq. (1) yields

$$\nabla\cdot(\mu\nabla u)=\frac{dp_d}{dx}\pm\rho_0\beta_0 g\Delta T(1-\beta_0\Delta T) \tag{5}$$

For the purpose of nondimensionalization of the momentum and energy equations, we wish to use the property values at the average temperature of the rod surface, denoted through suffix

Notation

A	Flow area, $\frac{1}{2}R^2(PDR^2\tan\theta_0-\theta_0)$
A^*	A/R^2
C_p	Specific heat at constant pressure, kJ/kg K
D_h	Hydraulic diameter, m
f	Fanning friction factor
G	Nondimensional pressure gradient, $\left(\frac{-dp_d}{dx}\right)\frac{R^2}{\mu_w u_{ref}}$
Gr	Grashof number, $\left(\frac{qR^4}{k_w}\cdot\frac{\beta_w g}{\nu_w^2}\right)$
g	Acceleration due to gravity, m/s^2
h	Convective heat transfer coefficient, W/m^2 K
k	Molecular thermal conductivity of the fluid, W/mK
k_r	Radiative conductivity, W/mK
$\dot m$	Mass flow rate, kg/s
$\dot m^*$	Dimensionless mass flow rate, $\dot m/\rho_w u_{ref}R^2$
Nu	Nusselt number, hD_h/k_w
n	Normal to a surface
P_t	Heat transfer perimeter, $(R\theta_0)$, m
P_w	Wetted perimeter, m
PDR	Pitch to diameter ratio
p	Axial pressure, Pa
QRC	Fraction of heat transferred by conduction
QRR	Fraction of heat transferred by radiation
q	Heat flux on the rod surface, W/m^2
q_r	Heat flux due to radiation exchange, W/m^2
R	Rod radius, m
Re	Reynolds number, $\dot m D_h/A\mu_w$
r	Radial coordinate, m
r^*	Dimensionless radial coordinate, r/R
T	Temperature, °K
T^*	Dimensionless temperature, $(T-T_0)/T_{ref}$
T_B	Bulk temperature, °K
T_0	Temperature at the cell-center, °K
T_{ref}	$qP_t/k_w\dot m^*$, °K
$\bar T_w$	Prescribed average temperature of the rod surface, °K
u	Local axial velocity, m/s
u^*	Dimensionless velocity, u/u_{ref}
u_{ref}	Dimensionless velocity $\left[=\left(\frac{-dp_d}{dx}\right)\frac{R^2}{\mu_w}\right]$, m/s
x	Axial coordinate, m
x^*	x/R
α	Coefficients for expressing a differential operator at a node through function values at neighboring nodes
β	Coefficient of thermal expansion, $-(1/\rho)(\partial\rho/\partial T)_p$, K^{-1}
θ	Angle, radian
θ_0	Included angle of a subchannel, radian
ε	Rod surface emissivity
ρ	Steam density, kg/m^3
κ_R	Rosseland mean absorption coefficient, (atm · m)$^{-1}$
τ_L	Optical thickness
τ_w	Wall shear stress, Pa
μ	Dynamic viscosity, Pa · s
ν	Kinematic viscosity, m^2/s

Superscripts and Subscripts

¯	Average value
*	Dimensionless value
d	Hydrodynamic
eff	Effective value
o	Corresponding to temperature T_0
R	Radiation
ref	Reference condition
s	Hydrostatic
w	Corresponding to average temperature of the rod surface $\bar T_w$

w, as reference conditions. Hence Eq. (5) becomes

$$\nabla\cdot(\mu^*\nabla u^*)=\frac{R^2}{\mu_w u_{ref}}\frac{dp_d}{dx}\pm\frac{R^2\rho_0\beta_0 g\Delta T}{\mu_w u_{ref}}(1-\beta_0\Delta T) \tag{6}$$

Setting $G=(R^2/\mu_w u_{ref})-(dp_d/dx)=1$ normalizes the momentum equation with respect to the imposed hydrodynamic pressure gradient and affords evaluation of u_{ref} in terms of dp_d/dx.

The thermal energy equation, including radiative transport, is

$$\rho c_p u\frac{\partial T}{\partial x}=\nabla\cdot(k\nabla T)-\nabla\cdot\vec{q}_r \tag{7}$$

Radiative transfer can take place between the rods and between a rod and the fluid surrounding it. However, in a symmetric arrangement, rod to rod heat exchange is absent if the decay-heat dissipated at each rod is the same. For fully developed thermal condition for uniform heat flux, input implies

$$\frac{\partial T}{\partial x}=\frac{dT_B}{dx}=\frac{qP_t}{\dot{m}c_p} \tag{8}$$

The rod to fluid radiative transfer can be evaluated from a knowledge of order of the opacity of the steam in the subchannel. The least characteristic length in a subchannel is $AB=(\mathrm{PDR}-1)R=L$, say. The Rosseland mean absorption coefficient $\kappa_R(T)$ for steam has a value of 328 $(\mathrm{atm}\cdot\mathrm{m})^{-1}$ at a typical temperature of 833 K.[18] Thus at 68 atm, the optical dimension of interest is

$$\tau_L=\kappa_R L=328\times 68\times 0.2\times 0.005\approx 22$$

for PDR = 1.2 and rod diameter of 10 mm. In other words, the medium is optically very thick, $\tau_L\gg 1$, and a diffusion model for radiation transfer is quite appropriate,[19]

$$\nabla\cdot\vec{q}_r=-\frac{16\sigma T^3}{3\kappa_R(T)}\nabla T=-k_r(T)\nabla T \tag{9}$$

At the surface, the expression for $k_r(T)$ should be multiplied by a factor of $(1-\varepsilon)/2$ to account for the fact that the surface is not black but has an emissivity ε.[20]

If as a first approximation, it is assumed the spatial thermophysical property variation can be accounted by writing, for example,

$$\bar{\mu}^*=\frac{1}{5}\sum_{i=0}^{4}\mu_i^* \tag{10}$$

where 1, 2, 3, and 4 are the nodes neighboring the focal point 0. Such averaging eliminates nonlinearity of the governing equations caused by transport property variations. Equation (6) is then rewritten as

$$\bar{\mu}^*\nabla^2 u^*=-G\pm\left(\frac{R^2\rho_0\beta_0 g\Delta T}{\mu_w u_{ref}}\right)(1-\beta_0\Delta T) \tag{11}$$

The energy equation (Eq. 7), together with Eqs. (8) and (9), can be written as

$$\bar{k}_{eff}^*\nabla^2 T^*=\frac{R^2 qP_t}{k_w T_{ref}}\left(\frac{\rho u}{\dot{m}}\right) \tag{12}$$

Introducing dimensionless temperature T^* and the area-averaged mass flow rate defined as

$$\dot{m}=\int_0^A\rho u dA=\rho_w u_{ref}R^2\int_0^{A^*}\rho^* u^* dA^* \tag{13}$$

permits Eq. (12) to be rewritten as

$$\bar{k}_{eff}^*\nabla^2 T^*=\left(\frac{qP_t}{k_w\dot{m}^* T_{ref}}\right)\rho^* u^* \tag{14}$$

Whereas q, P_t, and k_w are to be prescribed before commencing the solution of the governing equations, T_{ref} cannot be evaluated until $\dot{m}^*$ is estimated at the end of the computation. Temperatures can be determined only after the evaluation of T_{ref}. Moreover, whereas ρ^* and u^* vary from point to point, $\dot{m}^*$ is constant for given G, buoyancy, fuel rod emissivity, and average wall temperature conditions.

The buoyancy term in Eq. (11) can be rearranged as

$$\frac{R^2\rho_0\beta_0 g\Delta T}{\mu_w u_{ref}}(1-\beta_0\Delta T)=\left[\frac{\beta_w\rho_w g R^2 T_{ref}}{\mu_w u_{ref}}\right]\left(\frac{\rho_0}{\rho_w}\right)\left(\frac{\beta_0}{\beta_w}\right)T^*(1-\beta_0 T_{ref}T^*) \tag{15}$$

The term in the square brackets is simplified after substituting for T_{ref} and the definition of the Reynolds number as

$$\left(\frac{qR}{k_w}\cdot\frac{\beta_w g R^3}{\nu_w^2}\right)\left(\frac{\mu_w P_t}{\rho_w u_{ref}R^2\dot{m}^*}\right)=\mathrm{Gr}\left(\frac{P_t\mu_w}{\dot{m}}\right)=4\left(\frac{\mathrm{Gr}}{\mathrm{Re}}\right)$$

Both Reynolds and Grashof numbers are defined using the property values at the average temperature of the rod surface, which is considered known or can be evaluated otherwise, say, from the one-dimensional analysis of the thermal-hydraulic loop.

Considering that density and coefficient of thermal expansion of steam flowing through the rod bundle are inversely proportional to the temperature, we can now write the momentum equation (Eq. 11) as

$$\bar{\mu}^*\nabla^2 u^*=-G\pm 4\frac{\mathrm{Gr}}{\mathrm{Re}}\left(\frac{\bar{T}_w}{T_0}\right)^2 T^*\left[1-\frac{T_{ref}}{T_0}T^*\right] \tag{16}$$

and the energy equation (Eq. 14) as

$$\bar{k}_{eff}^*\nabla^2 T^*=\left(\frac{\bar{T}_w}{T}\right)u^* \tag{17}$$

It is useful to reiterate that Eqs. (16) and (17) have been derived by considering variation of thermophysical properties, including radiation transfer, and accounting for second-order changes in density in the buoyancy term. The radiation affects the momentum transport because of the coupling of the two governing equations through the buoyancy term. The value of $G=1$ can be chosen without loss of generality, thus normalizing the momentum equation.

These equations can be specialized to

(a) Boussinesq's approximation if the terms in parentheses in Eqs. (16) and (17) are set to unity.
(b) Variable properties, but first-degree buoyancy-dominated results are obtained when the term in square brackets in Eq. (16) is equated to unity.
(c) Constant property case is obtained by additionally setting $\bar{\mu}^*=1$ and $\bar{k}_{eff}^*=$constant.
(d) Constant property forced convection solution results by setting $\mathrm{Gr}=0$.
(e) If radiation transfer is not significant, $\bar{k}_{eff}^*=1$.

Thermophysical properties

The equation of state for steam at 68 bar and in the temperature range of 700 to 1000 K was found to follow the ideal gas law with a deviation of less than 5% and 1.5%, respectively, at the lowest and highest value of the temperature. Hence the steam density and thermal expansion coefficient were considered inversely proportional to temperature.

The fluid bulk temperature was evaluated accounting for variation of density as

$$T_B=\frac{\int\rho u T dA}{\int\rho u dA}\quad\text{or}\quad T_B^*=\frac{\int u^* dA^*}{\int(u^*/T^*)dA^*} \tag{18}$$

Hence

$$\dot{m}^*=-\left(\frac{\bar{T}_w}{T_b}\right)Q^* \tag{19}$$

The velocity and thermal conductivity of steam were correlated

for temperatures higher than 700 K to less than 1 % deviation as

$$\mu = 39.26 \times 100^{-6}(-0.6118 + 2.266\theta - 0.6547\theta^2)\ (\text{kg/ms}) \quad (20)$$

and

$$k = 0.0592(0.8302 - 0.0320\theta + 0.4903\theta^2)\ (\text{W/mK}) \quad (21)$$

The Rosseland mean absorption coefficient was approximated, using published results,[18] for different temperature ranges:

$$\kappa_R = 574.0(2.8 - 2.428\theta + 0.6286\theta^2)\ (\text{atm} \cdot \text{m})^{-1} \quad (22)$$

for $T < 1115$°K, where $\theta = T/555$, and

$$\kappa_R = 260\ (\text{atm} \cdot \text{m})^{-1} \quad \text{for } T > 1115\ \text{K} \quad (23)$$

Boundary conditions

The boundary conditions are

(a) $u^* = 0$ on the solid surface AD, $I = 1$.

(b) $\dfrac{\partial u^*}{\partial \theta} = \dfrac{\partial T^*}{\partial \theta} = 0$ along the symmetry lines AB, $J = 1$ and CD, $J = M$.

(c) Uniform heat flux on the rod surface:

$$\left.\frac{\partial T^*}{\partial r^*}\right|_{r^*=1} = -\frac{\dot{m}^*}{k^*_{\text{eff}_w}\theta_0} \quad (24)$$

(d) Along the symmetry line BC:

$$\frac{\partial u^*}{\partial n^*} = \frac{\partial T^*}{\partial n^*} = 0$$

Finite-difference equations and method of solution

The dimensionless momentum and energy equations (Eqs. 11 and 14) were solved simultaneously by a central difference scheme. The computation domain $ABCD$ (Figure 1a) was divided into a regular zone $ABED$ and an irregular zone BEC. The angular grids are $\Delta\theta$ apart in either zone. Radial grids are equidistant in the regular zone. In the zone BEC, arcs are drawn from the points of intersection of the symmetry line BC with the radius from 0. The distance, along a radius, between two consecutive arcs sets the radial grid length in the irregular zone.

At an inner node $0(i, j)$, the Laplacian is expressed as

$$\nabla^2\phi = \sum_{i=0}^{4} \alpha_i\phi_i \quad (25)$$

The coefficients α_i are evaluated by comparing the terms of $\nabla^2\phi$ with the Taylor's series expansions of ϕ_i at the neighboring nodes (Figure 1).

The difference forms of Eqs. (11) and (14) were solved simultaneously by a cyclic iteration process: from $I = 1$ to N and back from N to 1, J varying from 1 to M. The advantage of a cyclic iteration is that a node was traversed in both forward and backward marching, thus accelerating convergence.[16]

In the special case of constant properties and Boussinesq's assumption, solutions of Eqs. (11) and (14) need no input information other than the Gr/Re as a parameter. When effects of variable transport properties were sought, the value of average wall temperature, $\bar{T}_w$, had to be prescribed. The cases of $\bar{T}_w = 1000$ and 2000°K were tested for two values of rod surface emissivity, $\varepsilon = 0.5$ and 1.0. The value of T_0, which the reference density ρ_0 for the buoyancy term was based on, was chosen to be that prevailing at the top corner, point C, of Figure 1. The temperature at this point is expected to be the lowest owing to maximum convection effects. Thus $T_0 = T(N, M)$. Inclusion of second-degree variation in density due to buoyancy requires an input value for T_{ref} in Eq. (16). By definition, T_{ref} depends on the wall heat flux and the dimensionless mass flow rate $\dot{m}^*$, as well as the rod geometry and the knowledge of wall temperature. That is, second-degree buoyancy effects were investigated by prescribing a wall heat flux, typically $q = 2500\ \text{W/m}^2$. The evaluation of T_{ref} was kept inside the iteration loop so that the $\dot{m}^*$ value was updated at the end of each iteration.

Whereas satisfying condition (a) was of little difficulty, the gradient conditions (b) and (c) were satisfied by quadratic interpolations along the orthogonal grid lines. Imposition of zero gradient conditions along BC called for maximum care. We observed that the accuracy and convergence of the computed transport rates depended significantly on the extent condition (d) was satisfied at each of the intersecting node points.

The gradient at a node (Figure 1b) was expressed in terms of the Taylor's series expansions of the function at the neighboring points 1 to 5, following Greenspan,[21]

$$\frac{\partial\phi}{\partial n} = \frac{\partial\phi}{\partial r}\cos\theta - \frac{\partial\phi}{r\partial\theta}\sin\theta \quad (26)$$

and

$$\frac{\partial\theta}{\partial n} = \sum_{i=0}^{5} \alpha_i\phi_i \quad (27)$$

At the bottom and top corner, points B and C, all three gradient values are zero:

$$\frac{\partial\phi}{\partial r} = \frac{\partial\phi}{\partial\theta} = \frac{\partial\phi}{\partial n} = 0 \quad (28)$$

For the purpose of computation, each of the three gradients in Eq. (28) was added, and the general equation derived was satisfied at points B and C.

Five-point gradient interpolation was also adopted at nodes adjacent to point C.

Solution of the governing difference equations and application of the wall boundary condition afford evaluation of a calculated dimensionless average temperature of the wall:

$$\bar{T}^*_{w_c} = \frac{1}{M}\sum_{j=1}^{M} T^*(1, J) \quad (29)$$

On the other hand, the prescribed wall temperature, $\bar{T}_w$, can be written nondimensionally as

$$\bar{T}^*_w = \frac{\bar{T}_w - T(N, M)}{T_{\text{ref}}} \quad (30)$$

In the converged situation, values from Eqs. (29) and (30) should agree within prescribed limits, for example, 10^{-4}. The difference, $\bar{T}^*_{w_c} - \bar{T}^*_w$, was therefore, used as a correcting term in updating the nodal temperature value at the end of each iteration cycle:

$$T^*_{n+1}(I, J) = T^*_n(I, J) - (\bar{T}^*_{w_c} - \bar{T}^*_w) \quad (31)$$

where n denotes the iteration number.

A second independent and absolute test of convergence was recognized and adopted for forced flow (Gr/Re = 0). Under fully developed conditions,

$$\tau_w P_w = \left(-\frac{dp_d}{dx}\right)A$$

which results in

$$\frac{1}{M}\sum_{j=1}^{M}\left(\frac{\partial u^*}{\partial r^*}\right)_{I=1}\cdot\left(\frac{\theta_0}{A^*}\right) = \frac{R^2}{\mu_w U_{\text{ref}}}\left(-\frac{dp_d}{dx}\right) \quad (32)$$

The right-hand side of Eq. (32) is G by definition, and we have chosen $G = 1$ for computation. If we denote the left-hand side as GN, it simplifies that a converged forced flow solution should yield $GN = 1$.

The value of GN was computed and monitored for each of the geometries investigated for the case Gr/Re = 0. An agreement of better than 1 % was sought in each case by varying the grid size, relaxation factor, and initial values. The optimum values determined were then adopted for buoyancy- and radiation-dominated variable property solutions.

Table 1 Constant property forced convection results

(a) Triangular Array, $\theta=\pi$

		fRe					Nu		
Sl. No.	PDR	Oberjohn	Rehme	Dwyer *et al.*[23]	Sparrow *et al.*[7]	Present	Dwyer *et al.*[23]	Ramachandra[24]	Present
1	1.2	24.906	25.20	24.95	25.3	25.31	6.90	6.95	7.24
2	1.3	27.399	27.30	27.42	27.6	27.80	9.03	9.12	9.49
3	1.5	30.922	30.72	31.02	31.1	31.10	11.22	11.28	11.42
4	2.0	39.216	38.55	39.39	39.3	39.08	15.26	15.38	15.45

(b) Square Array, $\theta_0=\pi/4$

		fRe						Nu	
Sl. No.	PDR	Kim[25]	Oberjohn*	Meyder[26]	Rehme*	Present	Rehme[27]	Ramachandra[24]	Present
1	1.2	20.27	20.273	20.25	—	20.33	3.68	3.86	3.79
2	1.3	24.17	24.131	—	—	24.30	5.82	6.00	6.11
3	1.5	29.73	29.687	29.75	—	29.62	9.29	10.03	9.74
4	2.0	40.29	40.189	—	40.38	40.89	15.05	—	15.25

* W. J. Oberjohn and K. Rehme are cited by Johannsen.[22]

The initial values for temperature at different nodes were chosen as $T^*(1,J)=1.00$ and $T^*(I,J)=0.0$ for $I\neq 1$. The initial value for velocity had a marked influence on convergence. For a triangular array $\theta_0=\pi/6$ and PDR = 1.2 to 2 and a square array $\theta_0=\pi/4$ and PDR < 2, a good approximation for the initial velocity distribution was found to be

$$u^*(I,J)=\text{Haggen-Poiseulle profile}\times WF \quad \text{for } I\neq 1$$

where WF is a weighting factor that decreased from 1.75 to 1.25 as the PDR was increased from 1.2 to 2.0 with $\theta_0=\pi/6$. In case of $\theta_0=\pi/4$, the WF values decreased from 3.66 at PDR = 1.2 to 2.10 at 1.5. The optimum values were determined again by the convergence of the forced convection results. The Haggen-Poiseulle profile in case of buoyancy-dominated flow was evaluated, including the Gr/Re effects (Eq. 16). For PDR = 2.0 and $\theta_0=\pi/4$, a uniform velocity distribution $u^*(I,J)=1.0$, $I\neq 1$, was found to be a good initial choice.

Overrelaxation was found to generally accelerate convergence. Typically, $\Omega_u=1.5$ for velocity and $\Omega_T=1.2$ for temperature were good factors for forced convection in $\theta_0=\pi/4$ and PDR = 2.0, for which geometry the results could be compared with the results reported in the literature.

However, unequal relaxation factors resulted in unequal residues in u^* and T^*, especially when free convection effects were included. To eliminate any likely relaxation factor induced error, therefore, we chose $\Omega_u=\Omega_T=1.0$, which added by the cyclic iteration resulted in nearly equal residues for u^* and T^*, although at a relatively higher number of iterations of the order of 500. The residues at convergence were less than 10^{-5}.

Transport parameters

Fanning's friction factor for constant density fluid is defined through

$$-\frac{dp_d}{dx}=\frac{4f\rho u_{av}^2}{2D_h}$$

To account for density variation, we propose to write the above expressions as

$$-\frac{dp_d}{dx}=\frac{4f}{2D_h}\left(\frac{\dot m}{A}\right)^2\left(\frac{1}{\rho_w}\right) \tag{33}$$

where ρ_w is the density at average wall temperature, $\bar T_w$. On rearrangement, we get

$$f=\left(\frac{GA^*D_h^{*2}}{2\dot m^*}\right)\left(\frac{A\mu_m}{\dot m D_h}\right)$$

or

$$f\text{Re}=\frac{GD_h^{*2}A^*}{2\dot m^*} \tag{34}$$

Friction factors so obtained can then be used in Eq. (33) for estimating the pressure differential needed for a given flow rate $\dot m$ with prevailing wall condition in the geometry under consideration.

Heat transfer at the rod surface takes place due to the combined effects of molecular and radiative conductivities:

$$q=q_{cond}+q_{rad}=-(k_w+k_r)\left(\frac{\partial T}{\partial r}\right)_{r=R} \tag{35}$$

The ratios of molecular and radiative conduction to total heat flux are, respectively,

$$\text{QRC}=\frac{k_w}{k_w+k_r}=\frac{1}{k_{eff_w}} \tag{36}$$

and

$$\text{QRR}=1-\text{QRC} \tag{37}$$

The convective heat transfer coefficient, h, defined on the basis of conductive transport, expressed in dimensionless form is then

$$\text{Nu}=\frac{hD_h}{K_w}=\frac{\text{QRC}\,qD_h}{k_wT_{ref}(\bar T_w^*-T_B^*)} \tag{38}$$

After substituting for T_{ref} in Eq. (38), we obtain

$$\text{Nu}=\frac{\text{QRC}\,\dot m^*D_h^*}{\theta_0(\bar T_w^*-T_B^*)} \tag{39}$$

Results and discussion

Constant property forced convection

Computations were first conducted for the constant property, forced convection conditions so that the formulation could be tested by comparing it with the results available in the literature. In Table 1, we present the friction factor and heat transfer results for both triangular and square rod arrays along with typical information in the literature that our results are found to be in very good agreement with.

Parameter nomenclature

For the convenience of discussion, we have adopted the following nomenclature in presenting the results graphically. IDENS = 1 or 0 denotes, respectively, whether property variations are considered or not. The parameter $\beta=1$ or 2 indicates first- or second-degree density variation; IR = 0 or 1 when radiation is ignored or accounted for; $\varepsilon=1$ or 0.5, respectively, for two values of fuel rod surface emissivity. Numbering on the graphs follows the sequence IDENS, β, IR,

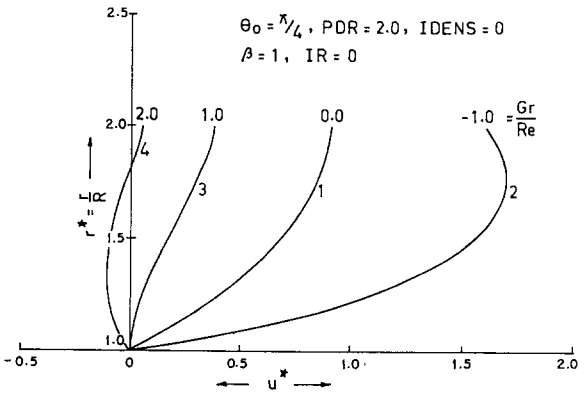

Figure 2 Effects of buoyancy on velocity profile along $J=1$, square array, PDR = 2.0

and ε. Subscript a denotes $\bar{T}_w = 1000°K$, and subscript b corresponds to $\bar{T}_w = 2000°K$.

Constant property buoyancy effects

When first-degree density variation is considered under Boussinesq's assumption, the momentum equation (Eq. 16) simplifies to

$$\nabla^2 u^* = -G \pm 4\left(\frac{\mathrm{Gr}}{\mathrm{Re}}\right) T^* \tag{40}$$

The dimensionless temperature T^* is ordinarily positive, since the reference temperature $T_0 = T(N, M)$ is likely to be the minimum in the flow domain. Since T^* is highest on the rod surface and decreases toward the maximum convection zone (BC in Figure 1a), the buoyancy effects decrease accordingly and ultimately vanish at $C(T^* = 0)$ for any value of Gr/Re. The forced flow potential is negative ($-G$) by definition. Buoyancy term in Eq. (4) assumes $+(\mathrm{Gr}/\mathrm{Re})T^*$ for downflow and $-(\mathrm{Gr}/\mathrm{Re})T^*$ for upflow. In other words, buoyancy effects support an upward main flow and oppose a downward flow.

Geometrically, the distance AB in Figure 1(a) marks the minimum flow area, and therefore, is a likely zone of extreme fluid temperature. For the purpose of quantitative comparison, we have hence, plotted representative velocity and temperature distributions along AB ($J=1$).

Figure 2 notes the effects of buoyancy on velocity profile in a square array ($\theta_0 = \pi/4$) with PDR = 2. The pure forced convection velocity profile (curve 1) is considerably enhanced in an upflow when Gr/Re = −1.0 (curve 2). The maximum is shifted to a lower radius because the buoyancy effect is felt most strongly closer to the wall. On the other hand, the buoyancy strongly reduces convection in downflow, as is observed in curves 3 and 4 for Gr/Re = 1.0 and 2.0. The flow is about to separate on the rod surface for Gr/Re = 1.0 and reversed for Gr/Re = 2.0.

The direct effect of velocity variation is on the subchannel average mass flow rate, which in turn, controls the fRe value through Eq. (34). A reduced $\dot{m}^*$ in downflow results in higher fRe value. Similarly, buoyancy reduces frictional resistance in upflow. Figures 3(a) and 3(b) show the variations for both triangular and square arrays. The increase in resistance is most pronounced for high PDR value and is less in case of a triangular array compared with a square arrangement.

The effects of reduced flow rate in downflow and increase in upflow due to buoyancy correspondingly reflect in the convective heat transfer rate (Figures 4a and 4b). Both in Figures 3(a) and 4(a), the buoyancy effects are negligible in a triangular array for PDR = 1.2 or 1.3. Since such PDR values are typical of the arrangements in a nuclear reactor, this observation is of considerable significance.

Variation of convection effects due to geometrical configuration results in highest rod surface temperature at A and smallest at D (Figure 1). These variations about the mean are ±0.25% for pure forced convection, increasing to ±1.5% at Gr/Re = 2.0 for PDR = 2.0 in a square array (Figure 5). For smaller pitch to diameter ratios, although buoyancy effects are less pronounced, the forced convection surface temperature deviates from isothermal condition to a more significant degree.

Variable properties, buoyancy, and radiation

Having generated the constant property pure forced convection and buoyancy-dominated transport rates, we carried out calculations, including effects of variable properties of steam at 68 bar, second-degree density changes due to buoyancy, and radiation transfer. The numbering of graphs in Figures 6–10 follow the nomenclature of Table 2. Apart from numerical identification, suffix a corresponds to a wall average temperature $\bar{T}_w = 1000$ K, and suffix b to $\bar{T}_w = 2000$ K.

Consider Figures 6(a) and 6(b) for friction factors in a square

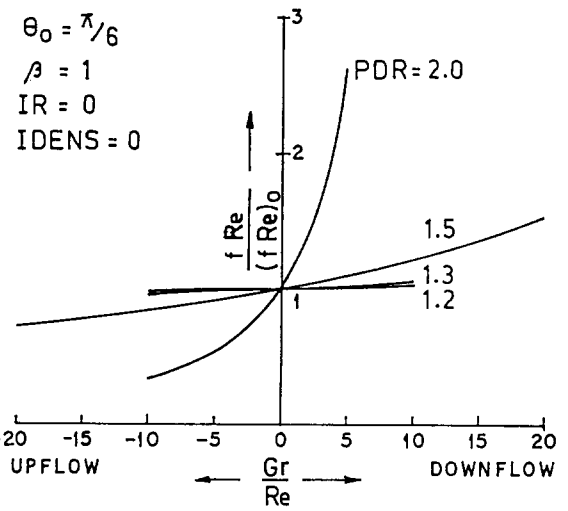

(a) Triangular array

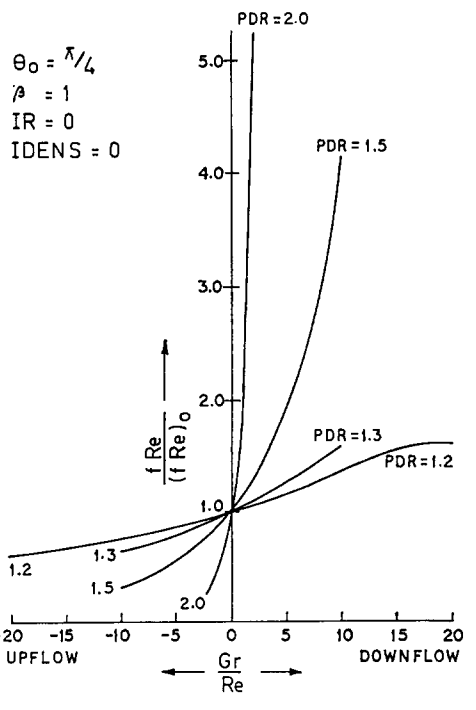

(b) Square array

Figure 3 Buoyancy effects on friction factor

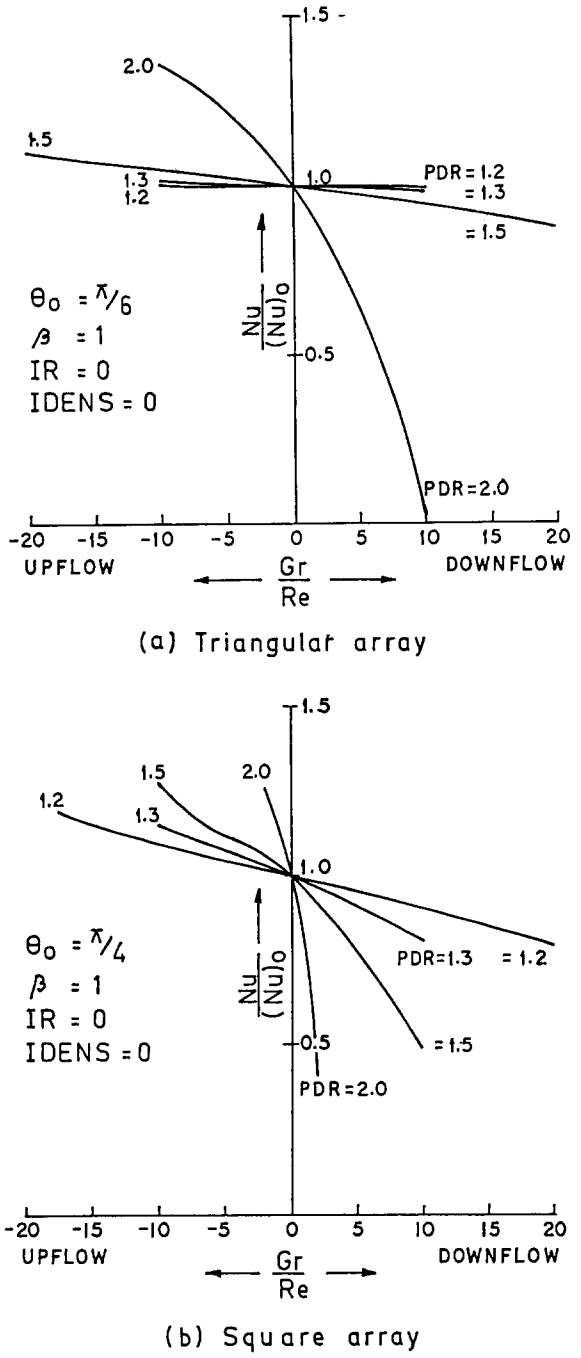

Figure 4 Effects of buoyancy on convective heat transfer

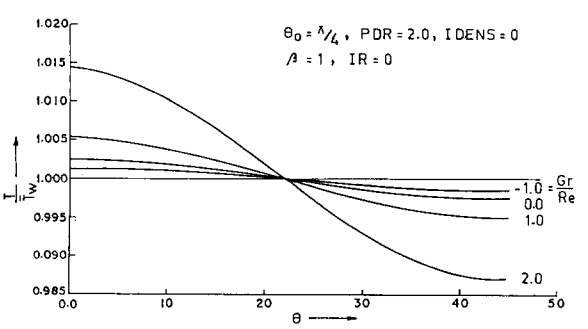

Figure 5 Rod surface temperature variations in a buoyancy-dominated flow through a square array, PDR=2.0

array of PDR = 1.3. Curves 1 and 2 are not much different from each other, indicating that second-degree density changes are not important for constant property solutions. On the other hand, examine curves 4a versus 1a and 4a versus 5a in Figure 6(a). The fRe value is increased from 38.47 to 94.63 when property variations are accounted for with $\beta = 1$ condition Gr/Re = 10.0. With Gr/Re = 2, the higher value is moderated to 74.61. However, when the wall temperature is taken as $\bar{T}_w = 2000°K$, curves 4b and 5b in Figure 6(b) indicate nearly equal value of 64.87. Apparently, with higher wall temperature, the relative variations of density are smaller. These observations call for a prescription of a threshold condition when second-degree density variation is warranted. We attempt an answer to this later.

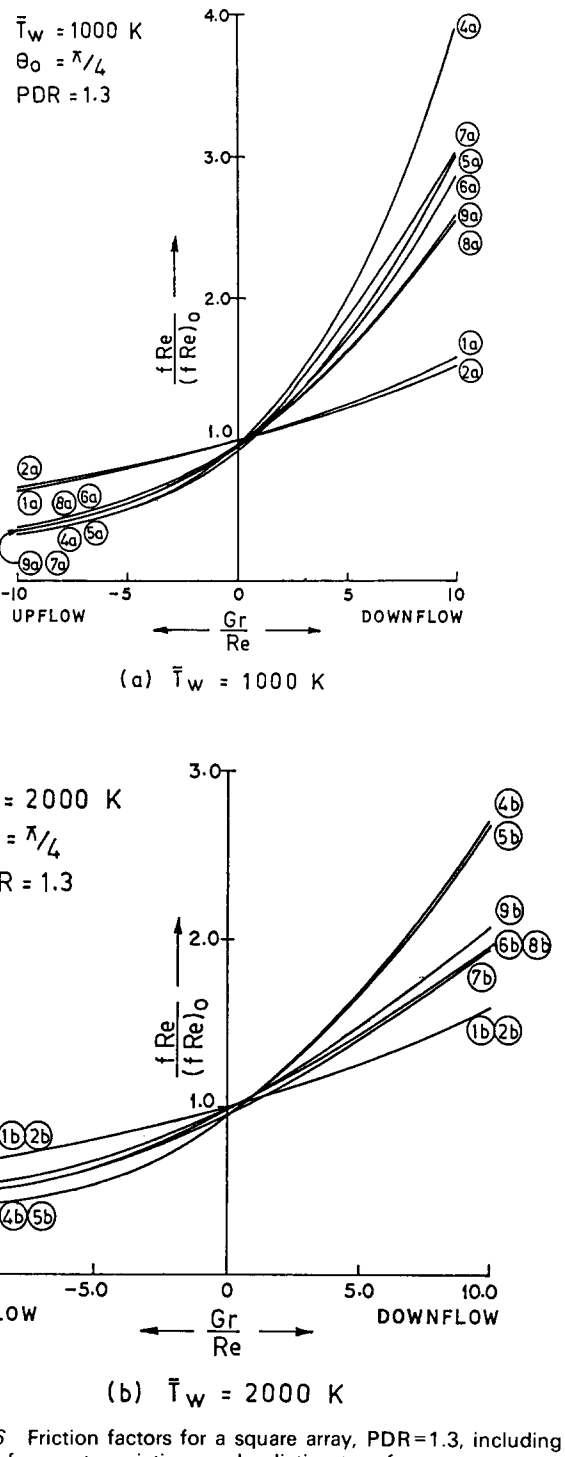

Figure 6 Friction factors for a square array, PDR=1.3, including effects of property variations and radiation transfer

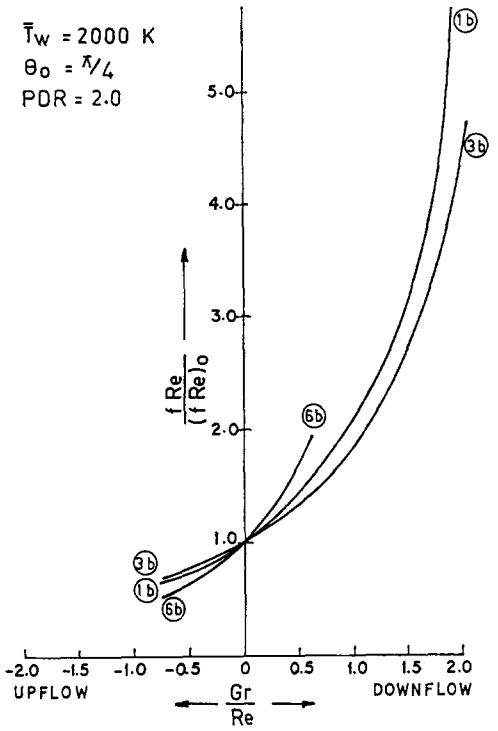

Figure 7 Effects of property variation, buoyancy, and radiation on fRe value in a square array, PDR=2.0, $\bar{T}_w$=2000 K

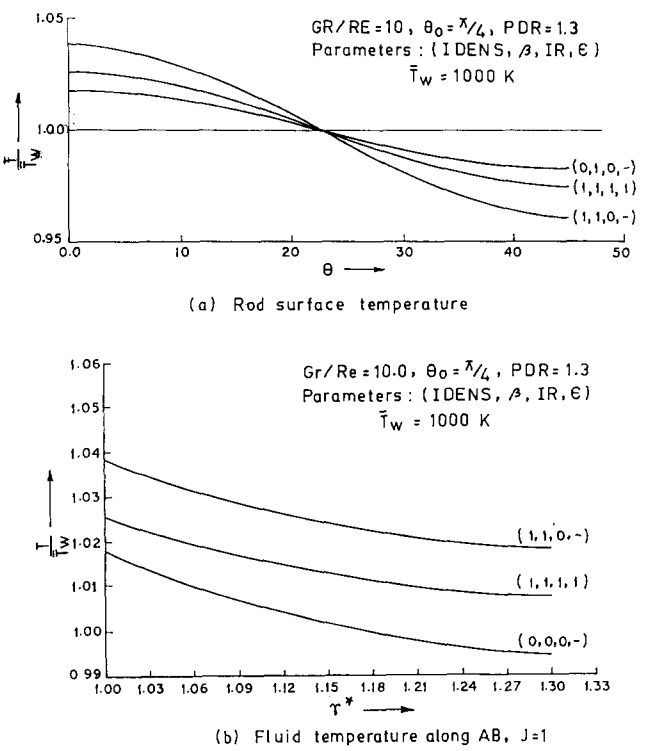

Figure 8 Effects of property variation, buoyancy, and radiation transfer on temperature, $\theta_0=\pi/4$, PDR=1.3

Radiation is parallel to convection and accounting for radiation transfer results in a more uniform temperature distribution and hence less severe buoyancy-related effects. Curves 3, 6, and 8 represent results for a black-clad surface, and curves 7 and 9 are for a gray-clad surface of $\varepsilon=0.5$. In both Figures 6(a) and 6(b), the fRe values are observed to be lower in the presence of radiation. We present representative fRe values for PDR=2.0, $\theta_0=\pi/4$, and $\bar{T}_w=2000$ K in Figure 7 without further explanation.

The effects of property variation, buoyancy, and radiation transfer on the rod and fluid temperature can be noted from representative plots in Figures 8(a) and 8(b). The hot spot temperature is 1038 K for $\bar{T}_w=1000$ K if only property variation and buoyancy are accounted for. The temperature moderates to 1025 K if radiation transfer is considered.

The influence of IDENS = 1, $\beta=2$, IR = 1 on Nusselt numbers is opposite to those of fRe following the discussion for constant property buoyancy effects. In Figures 9(a) and 9(b), we have presented the convective heat transfer coefficients for $\bar{T}_w=1000°$ and 2000°K, respectively. Whereas fRe depends solely and inversely on the variation of $\dot{m}^*$ (Eq. 34), Nu varies directly with $\dot{m}^*$ and inversely with $(\bar{T}_w^*-T_B^*)$ (Eq. 39). Thus the difference between Nusselt numbers is moderate compared to the fRe results. A high $\bar{T}_w$ value obviously would moderate the variation still further (compare Figures 9a and 9b).

By virtue of Eqs. (36) and (37), the radiation component of total heat transfer was constant for a given value of $\bar{T}_w$ and ε. Radiation accounted for 14.2% at $\bar{T}_w=1000$ K for $\varepsilon=1$, reducing to 11.0% with $\varepsilon=0.5$. The two values at $\bar{T}_w=2000$ K

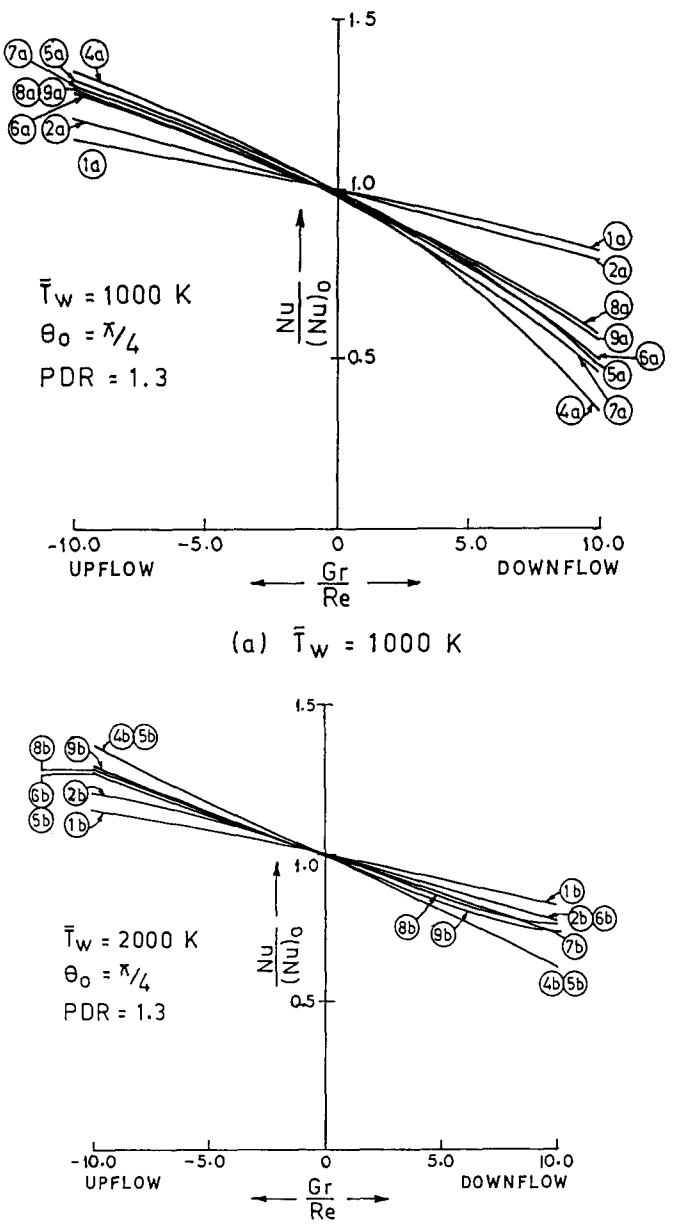

Figure 9 Convective heat transfer under variable property, buoyancy, and radiation transfer conditions, $\theta_0=\pi/4$, PDR=1.3

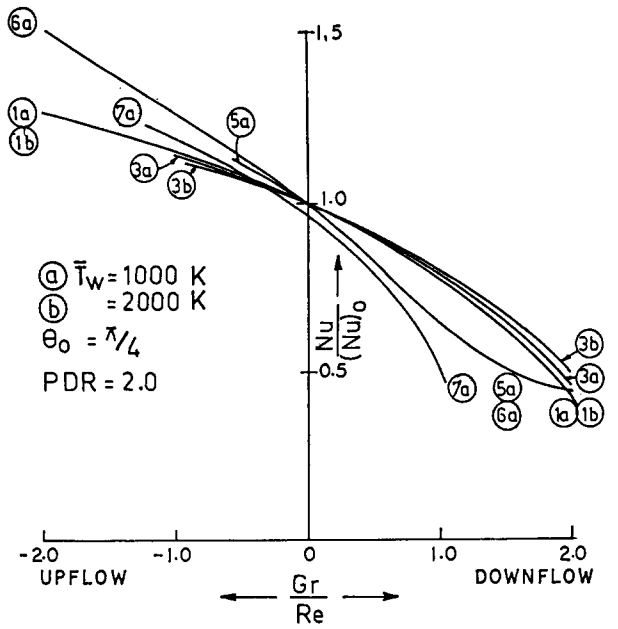

Figure 10 Nusselt number variations due to IDENS, β, and IR in a square array, PDR=2.0

Table 2 Nomenclature for graph numbering

Curve No.	IDENS	β	IR	ε
1	0	1	0	—
2	0	2	0	—
3	0	1	1	1.0
4	1	1	0	—
5	1	2	0	—
6	1	1	1	1.0
7	1	1	1	0.5
8	1	2	1	1.0
9	1	2	1	0.5

were 29.9% and 24.3%, respectively. Recall that the transport rates in a triangular array with PDR = 1.2 and 1.3 remained practically invariant when constant property buoyancy effects were considered (Figures 3a and 4a). We noticed similar invariance, within limits of $\pm 5\%$, for $\theta_0 = \pi/6$ and PDR = 1.3, even when property variations and radiation transfer were accounted for.

The influence of IDENS, β, and IR is significant for PDR = 2.0 and $\theta_0 = \pi/4$, for which we present the convective heat transfer coefficients in Figure 10.

Limits of first-degree density variation

As noted, accounting for second-degree density change becomes necessary when the wall temperature is lower (for example, $\bar{T}_w = 1000$), buoyancy is significant in downward flow (for example, Gr/Re = 10), and property variations are considered, but radiation may be neglected.

To establish a general criterion for including $\beta = 2$ effects, we attempted to summarize the Nusselt numbers for all situations computed in this study. Since density change is linked to temperature difference, we chose $[(T_w - T_B)/T_w]$ as the independent parameter and plotted the ratio $(Nu_{\beta=2}/Nu_{\beta=1})$ in Figure 11. The Nusselt number ratio was calculated for a pair of parameters, where all parameters except the β value were identical.

The plots in Figure 11 indicate second-degree density changes can be neglected in upflows, (Gr/Re) < 0. In downflows, however, the second-degree change begins to reflect as early a temperature difference as $(\bar{T}_w - T_B) = 10$°K at $\bar{T}_w = 1000$°K, especially if property variations are included. The correction of Nusselt number is as much as 30% for $\beta = 2$ compared to $\beta = 1$ of IDENS = 1 [at $(\bar{T}_w - T_B) = 100$ K]. The convection is lower by 6% for the same value of ΔT if property variations are neglected.

Since the results presented in Figure 11 have been generated by considering several geometric and thermal conditions, it may be plausible to apply these results to laminar convection in other geometries as well. The information can be used as follows. First, evaluate Nu and T_B for a given T_w geometry and Gr/Re, considering $\beta = 1$. Compute $(\bar{T}_w - T_B)/\bar{T}_w$, and if the value exceeds the threshold limit, apply $\beta = 2$ correction to Nu from Figure 11. The bulk temperature may then be recalculated. The two curves, IDENS = 0 and 1 in Figure 11 also quantitatively indicate the penalty for ignoring property variations in a downflow. At $(\bar{T}_w - T_B) = 30$ K, the property variation causes a 4% rise in Nu, whereas the rise is about 16% at 90 K temperature difference on a $\bar{T}_w = 1000$ K base.

Conclusions

We undertook this numerical study of laminar, combined free, and forced convection together with radiation transfer in square and triangular arrays with the primary objective of obtaining transport rates for a PWR under LOCA condition. Although the PDR value of interest for a PWR is small, that is, 1.2 or 1.3, we have generated results for higher values for completeness. The fluid is taken to be steam at 68 bar whose thermophysical properties are considered variable. High optical dimension, of the order of 20 for a low PDR = 1.2, permits applying a diffusion model for radiation transfer.

The buoyancy effect supports an upward flow and opposes a downward flow. Thus the flow rate and convective heat transfer are enhanced and friction factor reduced in upflow due to buoyancy. Reverse effects are observed in downflow, where typically, flow separation and backflow can be encountered at high Gr/Re value, especially in a square array with high PDR value. Fortunately, buoyancy causes less variation at smaller PDR values of 1.2 and 1.3. Transport rates in a triangular array and low PDR are practically insensitive to buoyancy effects.

Transport rate variations in a square array, even at low PDR, are sensitive to effects of fluid property variation, especially in downflow. Typically, the fRe value with property variations for PDR = 1.3, $\theta_0 = \pi/4$, Gr/Re = 10.00, $\beta = 1$ was found to be about two and a half times the constant property value. Radiation transfer between the fuel rod and the fluid reduces temperature variation in the coolant and thereby moderates the effects of buoyancy and property changes.

The heat transfer rate for $\theta_0 = \pi/4$, PDR = 1.3 by radiation is about 14% of the total at $\bar{T}_w = 1000$ K. The rate increases to 30% at 2000 K, assuming the fuel rod surface to be black.

Boussinesq's approximation can be accepted in most situations involving buoyancy in upflow. In downflow,

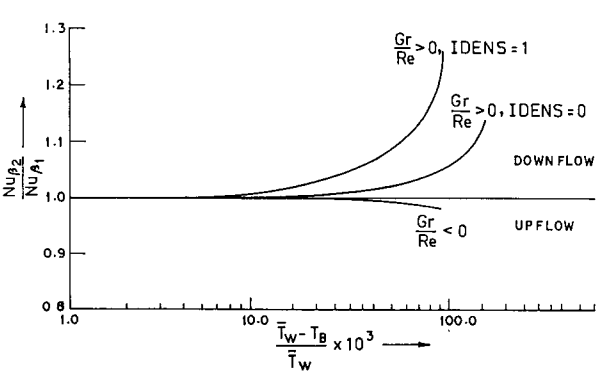

Figure 11 Second-degree buoyancy effects on Nusselt number

however, second-degree density changes account for the increase in Nusselt number by 6% compared with constant properties and nearly 30% with variable properties when wall to bulk temperature difference is 10% of the average wall temperature. In other words, Boussinesq's assumption gives a conservative estimate of convective heat transfer coefficients for a heat dissipating surface subjected to fluid flow in the downward direction.

In this study, the reference conditions, including the thermophysical properties for defining Re, Gr, and Nu, have been taken at the average temperature of the wall for convenience in applying the results.

Acknowledgments

This work was done, in part, when one of the authors (A.K.M.) held a visiting appointment at Purdue University. He would like to gratefully acknowledge the authorities of Indian Institute of Technology, Kharagpur, for sanctioning a leave of absence. The present study was supported in part by the Electric Power Research Institute under Project 1760-3.

References

1 Collier, J. G. and Davis, L. M. The accident at Three Mile Island. *Heat Transfer Eng.*, 1980, **1**, 56–67

2 Nuclear Regulatory Commission Special Inquiry Group. Three Mile Island, a report to the commissioners and to the public. U.S. Nuclear Regulatory Commission, Washington, D.C., 1980, Vol. II, Part 2

3 Viskanta, R. and Mohanty, A. K. TMI-2 accident: postulated heat transfer mechanisms and available data base. U.S. Nuclear Regulatory Commission, Washington, D.C., 1981, NUREG/CR-2121 (ANL-81-26)

4 Viskanta, R. and Mohanty, A. K. Effects of zircaloy oxidation and steam dissociation on cooling of a PWR core under conditions simulating uncovered fuel rods. Electrical Power Research Institute (in press)

5 Pien, S. J. and Chao, B. T. The coupling of hydrogen generation and thermal hydraulics in reactor core under uncovering conditions. Interim Report Submitted to Electric Power Research Institute, Sept. 1983

6 Viskanta, R. and Kim, D. M. Heat transfer in a partially uncovered reactor core. *Nucl. Eng. Design*, 1985, **85**, 71–82

7 Sparrow, E. M. and Loeffler, A. L., Jr. Longitudinal flow between cylinders arranged in a regular array. *AIChE Journal*, 1959, **51**, 325–329

8 Sparrow, E. M., Loeffler, A. L., Jr. and Hubbard, H. A. Heat transfer to longitudinal laminar flow between cylinders. *J. Heat Transfer*, 1961, **83**, 415–422

9 Shah, R. K. and London, A. L. Laminar flow forced convection in ducts. *Advances in Heat Transfer*, Supplement I. Academic Press, New York, 1978

10 Kakac, S., Shah, R. K. and Bergles, A. L. *Low Reynolds Number Flow Heat Exchanger*. Hemisphere Publishing Corp., New York, 1982

11 Iqbal, M., Ansari, S. A. and Aggarwala, B. D. Buoyancy effects on longitudinal laminar flow between vertical cylinders arranged in regular arrays. *Heat Transfer 1970*, Vol. IV, Paper No. C3.6, Elsevier, Amsterdam, 1970

12 Iqbal, M., Aggarwala, B. D. and Khatmy, A. K. On the conjugate problem of laminar combined free and forced convection through vertical noncircular ducts. *J. Heat Transfer*, 1971, **93**, 52–56

13 Ramm, H. and Johannsen, K. Combined forced and free laminar convection in vertical rod bundles with longitudinal flow. ASME Paper No. 77-HT-44, 1977

14 Yang, J. W. Analysis of combined convection heat transfer in infinite rod arrays. *Heat Transfer—1978*, Vol. 1. Hemisphere Publishing Corp., Washington D.C., 1978, 49–54

15 Yang, J. W. Heat transfer and fluid flow in regular rod arrays with opposing flow. *Fluid Flow and Heat Transfer Over Rod or Tube Bundles*, ed. S. C. Yao and P. A. Pfund. ASME, New York, 1979, 149–153

16 Das, R. and Mohanty, A. K. Laminar combined convection in finite circular rod bundles. *J. Heat Transfer*, 1984, **106**, 563–569

17 Zhong, Z. Y., Yang, K. T. and Lloyd, J. R. Variable property effects in laminar natural convection in a square enclosure. *J. Heat Transfer*, 1985, **107**, 133–138

18 Abu-Romia, M. M. and Tien, C. L. Appropriate mean absorption coefficients for infrared radiation of gases. *J. Heat Transfer*, 1967, **89**, 321–327

19 Viskanta, R. Radiation transfer and interaction of convection with radiation heat transfer. *Advances in Heat Transfer*, ed. T. F. Invine, Jr. and J. P. Hartnett, Vol. 3. Academic Press, New York, 1966, 175–251

20 Deissler, R. G. Diffusion approximation for thermal radiation in gases with jump boundary condition. *J. Heat Transfer*, 1964, **86**, 240–246

21 Greenspan, D. *Introductory Numerical Analysis of Elliptic Boundary Value Problems*. Harper International Edition, New York, 1965

22 Johannsen, K. Longitudinal flow over tube bundles. *Low Reynolds Heat Exchangers*, ed. S. Kakac *et al.* Hemisphere Publishing Corp., Washington, D.C., 1983, 229–273

23 Dwyer, O. E. and Berny, H. C. Laminar flow heat transfer for in-line flow through unbaffled rod bundles. *Nuclear Science and Engineering*, 1970, **42**, 81–88

24 Ramachandra, V. and Spalding, D. B. The numerical prediction of laminar heat transfer in rod-bundle geometries. HTS/78/4, Imperial College, Heat Transfer Section, London, 1978

25 Kim, J. H. Heat transfer in longitudinal laminar flow along circular cylinders in square array. *Fluid Flow and Heat Transfer Over Rod or Tube Bundles*, ed. C. Yao and P. A. Pfund. ASME, New York, 1979, 155–161

26 Meyder, R. Solving the conservation equations in fuel rod bundles exposed to parallel flow by means of curvilinear-orthogonal coordinates. *J. Comp. Phys.*, 1975, **17**, 53–67

27 Rehme, K. Institut fur Neutroneuphysik und Reaktortechnik, Karlsruhe, West Germany, personal communication, 1985